

Title No. 119-M16

Mechanical Behavior and Design Properties of Ultra-High-Performance Concrete

by Rafic G. El-Helou, Zachary B. Haber, and Benjamin A. Graybeal

The appropriate and efficient design of structural components made with ultra-high-performance concrete (UHPC) requires the establishment of key design properties and material models that engage UHPC's distinct mechanical properties, as compared to conventional concrete. This paper presents the results of an extensive program of compression and tension property assessment executed according to existing testing methods to assess the mechanical characteristics of several commercially available UHPC products. The experimental results are then used to propose suitable mechanical models and design parameters that are foundational for the structural-level application of UHPC. The models rely on a set of experimentally identified mechanical performance properties that distinguish UHPC from conventional concrete and establish the basis of the material qualification for use in structural design. As such, this work constitutes a fundamental step in ongoing efforts to develop UHPC structural design guidance in the United States.

Keywords: compression properties; mechanical models; structural design parameters; tension properties; ultra-high-performance concrete (UHPC).

INTRODUCTION

A new class of cementitious materials known as ultra-high-performance concrete (UHPC) offers distinct mechanical and durability properties, creating opportunities for new construction while necessitating novel design frameworks. Composed of a dense cementitious matrix with a disconnected pore network, and reinforced with a heavy dosage of high-strength steel fibers, UHPC is characterized by very low permeability, high compressive strength, and sustained tensile resistance.¹⁻⁷ In recent years, many UHPC-class materials have been developed, offering flowable, self-consolidating solutions optimized for structural applications and exhibiting compressive strengths exceeding 124 MPa (18.0 ksi).⁸⁻¹⁰ More importantly, these concretes demonstrated superior tensile and durability characteristics compared to other fiber-reinforced composites, as UHPC-class materials can provide a sustained post-cracking tensile resistance of more than 5 MPa (0.73 ksi) coupled with exceptional crack control.¹¹⁻¹⁶ With UHPC, a cementitious composite can now be designed to withstand substantial tensile strain, and by employing design principles suited for this distinctive material behavior, new forms of concrete construction can be unlocked, offering savings in material use through the reduced reliance on traditional steel reinforcement, as well as reduced member dimensions, concrete cover, and dead loads.^{17,18} In the United States, these benefits are beginning to be realized through deployments of UHPC in several highway bridge construction projects since 2006.^{19,20} Although more than 250 bridges in the United

States have used UHPC, most of these deployments focused on small-scale applications—for example, connections between prefabricated bridge elements replacing conventional cementitious grouts.^{13,21} The implementation of full-scale structural components has been limited, given the lack of design guidance that allows for the use of the enhanced properties in the design process.

Concrete bridge design in the United States is reliant on the material models and design provisions of the American Association of State Highway and Transportation Officials (AASHTO) Load and Resistance Factor Design (LRFD) Bridge Design Specifications.²² These provisions are not suitable for design with UHPC, as they do not facilitate use of the enhanced material behavior on the structural performance level, leading to inefficient and overly costly UHPC structures. To address this need, the Federal Highway Administration (FHWA) has embarked on an effort, coordinated with the AASHTO Committee on Bridges and Structures, to develop the needed UHPC structural design guidance. Although tailored for bridge applications, the fundamentals of the design approach are applicable to a wide range of structural solutions outside the realm of highway bridges. The proposed design process is founded on first principle approaches, where key material-level performance characteristics are experimentally identified through appropriate material testing and linked to the structural-level performance through structural mechanics and design models.

The objective of the research presented in this paper is to investigate the fundamental characteristics of UHPC material behavior in compression and tension and propose mechanical models for use in structural design. An emphasis on the material performance metrics that distinguish UHPC from conventional concrete are identified throughout the manuscript, which are then used to propose threshold material parameters that qualify a UHPC material for use in structural design. These parameters are determined based on a large set of experimental data obtained by conducting tests to assess the characteristics of several UHPC products available in Europe and North America.

ACI Materials Journal, V. 119, No. 1, January 2022.

MS No. M-2020-522.R2, doi: 10.14359/51734194, received June 23, 2021, and reviewed under Institute publication policies. Copyright © 2022, American Concrete Institute. All rights reserved, including the making of copies unless permission is obtained from the copyright proprietors. Pertinent discussion including author's closure, if any, will be published ten months from this journal's date if the discussion is received within four months of the paper's print publication.

BACKGROUND

A key starting point in structural design is the determination of material-level properties and mechanical models that appropriately describe the material's intrinsic response when subjected to structural loads. Testing of these properties and their associated mechanical models are established for conventional concrete and delineated in AASHTO LRFD Bridge Design Specifications.²² For instance, the compression parameters—namely, the compressive strength and elastic modulus—are obtained by executing ASTM C39²³ and ASTM C469,²⁴ respectively. These parameters are then used to inform the structural design tools and predict the capacities of concrete members. At service loads, the compression stress-strain behavior is described by a linear response with a slope equal to the elastic modulus. At ultimate limit state, a calibrated equivalent rectangular stress block is permitted to be used in lieu of the actual stress-strain distribution. Nevertheless, the use of strain-based analytical methods that mimic the experimental concrete stress-strain behavior is permitted and recommended in many cases—for example, determining the flexural capacity of a composite section made of different concretes. In tension, concrete offers a negligible resistance, which is often ignored in structural design. Instead, discrete steel reinforcements are added and proportioned to carry all tensile loads and control cracking. Moreover, given the low value of the concrete tensile response, direct measurements are difficult to capture, and designers often revert to indirect measurement procedures, such as the determination of modulus of rupture, in accordance with AASHTO T 97²⁵ or ASTM C78.²⁶

The material behavior of UHPC is fundamentally different from conventional concrete. UHPC offers a sustained post-cracking tensile resistance and tight crack spacing without any auxiliary steel reinforcement. In compression, UHPC's expected capacities exceed the range of strength values for which conventional concrete structural design guidance was developed; AASHTO LRFD provisions were developed for materials with compressive strength values below 68.9 MPa (10.0 ksi), and in specific articles, the provisions are applicable up to compressive strength values of 103 MPa (15.0 ksi).²² To address the lack of structural design guidance for UHPC and materials offering sustained post-cracking tensile resistance, many countries around the world have developed new guidance specifically for structural members made of these emerging materials.²⁷⁻³⁵ Of note are the French, Swiss, and Canadian UHPC design guidance documents.²⁷⁻³¹ The approach followed in these recommendations first delineates threshold values for key material properties that characterize UHPC-class materials; second, outlines new testing protocols to obtain those properties; and third, associates the material behavior to suitable mechanical models used in the design process. In France, a UHPC shall only be used in primary load-bearing components if it is reinforced with metallic fibers, exhibits a characteristic compressive strength between 150 and 250 MPa (21.8 and 36.3 ksi) and a minimum characteristic tensile strength of 6 MPa (0.9 ksi), delivers sufficient ductile behavior in flexure by satisfying a prescribed stress versus crack opening threshold, and has a density between

2300 and 2800 kg/m³ (143.6 and 174.8 lb/ft³). In Switzerland, the minimum compressive limit for structural-grade UHPC is set at 120 MPa (17.4 ksi). However, the tension response is mandated to exhibit a strain-hardening behavior with a minimum cracking stress value of 7.0 MPa (1.0 ksi) and an ultimate capacity of at least 7.7 MPa (1.1 ksi), achieved at a uniaxial tensile strain value greater than 0.0015. In Canada, the minimum compressive strength is also set at 120 MPa (17.4 ksi), and tension-hardening UHPC must exhibit minimum cracking and ultimate strength values of 5.0 and 5.5 MPa (0.7 and 0.8 ksi), respectively, with sustained post-cracking strain values greater than 0.001.

The test methods and associated design models vary between the French, Swiss, and Canadian recommendation documents. In compression, each jurisdiction adopted a modified version of the existing test method already in place for conventional concretes. The French standard allows the usage of two stress-strain relationships to describe the compressive behavior. The first relationship mimics the experimental curve in its linear, nonlinear, and post-peak regimes until the post-peak strength decreases by 30% from its ultimate strength value. The second model simplifies the response using an elastic-plastic representation with reduced design strength and ultimate strain values. In contrast, the Swiss design recommendation characterizes UHPC for design by a linear stress-strain relationship until the compressive strength is reached, while the Canadian recommendation allows the use of a rectangular stress block distribution at ultimate limit state. For tension testing, the French developed rigorous inverse analysis techniques to back-calculate the uniaxial tensile stress-strain trends from flexural prisms tested in three-point (notched and unnotched) and four-point (unnotched) bending. These techniques rely on specified procedures involving analytical assumptions and empirical formulations to account for the gradient effect and estimate curvatures based on the measured vertical deflection of the beam. The tension models described for structural design are: 1) an elastic-plastic stress-strain representation for tensile hardening where the stress after cracking is maintained with increasing strain; 2) bilinear stress-strain tensile hardening where the stress continues to increase with increasing strain after cracking; and 3) tensile-softening behavior accounting for post-localization stresses, only allowed to be used in thick, structural members. In Switzerland, tensile-hardening materials showing a clear increasing stress after cracking are solely permitted and represented in a bilinear stress-strain model. The experimental uniaxial tensile behavior can be obtained either from a direct tension test for UHPC or from an inverse analysis method of flexural prisms tested in four-point bending. In Canada, the tensile properties can be obtained from inverse analysis techniques specified in the Canadian, French, or Swiss design recommendations, or from a published direct tension method. A bilinear strain model for tension-hardening UHPC is specified. Table A-1 of Appendix I* presents a synopsis of the

*The Appendix is available at www.concrete.org/publications in PDF format, appended to the online version of the published paper. It is also available in hard copy from ACI headquarters for a fee equal to the cost of reproduction plus handling at the time of the request.

specified test methods in each of the three international recommendation documents, along with a list of typical values indicative of UHPC mechanical behavior.

Many research efforts in the United States and Canada have focused on characterizing the mechanical behavior of UHPC and developing standardized test methods for this class of material to facilitate the use of UHPC in structural design. These efforts have led to the publication of a new ASTM International standard: ASTM C1856, Standard Practice for Fabricating and Testing Specimens of Ultra-High Performance Concrete.³⁶ The standard covers sampling and testing of fresh UHPC, making and curing of test specimens, and testing of hardened properties, including compressive strength, static modulus of elasticity, Poisson's ratio, and flexural strength, among others; the standard also prescribes modifications to existing ASTM standards to make them applicable to UHPC-class materials. Although the standard covers the testing to assess key characteristics of UHPC material behavior, it does not address the uniaxial tensile characteristics that are central to any structural design guidance development effort. Existing direct or indirect tensile strength testing methods for conventional concretes and mortars (for example, the modulus of rupture test²⁶ and splitting tensile tests³⁷) are designed to classify brittle materials, resulting in overestimation of tensile strength capacities if applied without appropriate analysis procedures to materials exhibiting stable post-cracking tensile deformation. To obtain UHPC tensile properties, researchers often rely on uniaxial tension testing methods³⁸⁻⁴³ or revert to analytical assumptions and empirical approximations to estimate the uniaxial response from flexural tests.⁴⁴⁻⁴⁸ Graybeal and Baby⁴⁹ developed a straightforward method to directly characterize the tension behavior of UHPC based on test methods commonly used for characterizing metals. This method has been recently adopted as an AASHTO standard method of test: AASHTO T 397, Standard Method of Test for Uniaxial Tensile Response of Ultra-High Performance Concrete.⁵⁰ The work detailed herein adopts the aforementioned test method for its proven ability to: 1) accurately capture the uniaxial tensile mechanical response without the need of empirical assumptions associated with inverse analysis methods of flexural prisms; and 2) examine both cast and extracted specimens without requiring the use of milling or machining, thus facilitating studies of tensile response properties of in-place UHPC.

RESEARCH SIGNIFICANCE

The appropriate and efficient design of UHPC structural solutions requires a thorough understanding of the material-level performance and design models that properly use these properties in the design process. This paper presents an extensive set of experimental investigations performed by the authors of the compression and tension behavior of commercial UHPC products. The data are then used to propose appropriate mechanical models for use in the design process and to identify minimum performance metrics that distinguish UHPC material properties from other cementitious composites. As such, the work provides fundamental

information to support ongoing efforts to develop UHPC structural design guidance in the United States.

EXPERIMENTAL INVESTIGATION

The experimental program presented herein consists of a total of 492 cylindrical specimens tested in uniaxial compression and 190 prismatic specimens tested in uniaxial tension with the primary goal of obtaining a range of indicative values of UHPC material characteristics. The examined properties include modulus of elasticity, compressive strength, strain at peak compressive strength, Poisson's ratio, tensile cracking strength, strain at crack localization, and tensile capacity.

UHPC-class materials

Eleven commercial UHPC products developed by nine suppliers in Europe and North America were part of this study. Because the materials are proprietary, information about the type and proportions of powder constituents (for example, cement, silica fume, ground quartz, and fine sand) were not disclosed. The products were delivered in three primary constituents: preblended powder mixture containing all the granular constituents, liquid admixtures, and commercially available steel fiber reinforcement. Table A-2 of Appendix II lists the mixture design proportions for each UHPC-class material. When several products are provided by the same supplier, each product is assigned a numerical identifier, as shown in Table A-2.

UHPC specimens were dosed with their recommended proportion of discontinuous steel fibers, and with varying fiber proportions ranging between 1.00 and 4.50% by volume to investigate the effect of fiber reinforcement ratio on the mechanical properties. The fibers were supplied by the UHPC manufacturer and varied in length, shape, diameter, and tensile strength. The manufacturer-reported properties of the fibers used in each UHPC material are listed in Table A-3 of Appendix II. All the steel fibers considered were brass-coated with a minimum specified tensile strength greater than 2100 MPa (304.6 ksi), except for products F-A and F-F, which did not have any coating and had a tensile strength of 1100 and 689 MPa (159.5 and 100 ksi), respectively. Fiber F-P was made of polyvinyl alcohol (PVA) and had a tensile strength of 1000 MPa (145.0 ksi). Most suppliers used one type of fiber product in their mixture designs, while two suppliers (U-B and U-G) recommended a blend of two fiber volume fractions, as shown in Table A-2.

The batching of the UHPC constituents was performed according to manufacturer recommendations at the FHWA Turner-Fairbank Highway Research Center (TFHRC) research laboratories. Most specimens were cured in ambient laboratory conditions, while a few were subjected to steam-like conditions soon after casting to accelerate property development. A subset of the specimens made of materials U-H2 and U-J1, denoted by U-H2b and U-J1b, were part of a larger experimental study of prestressed UHPC girders and were batched and cast at two different precast plants and stored outdoors next to the UHPC associated girders until the girders and specimens were delivered to TFHRC. Specimens made of material U-H2b were covered and subjected

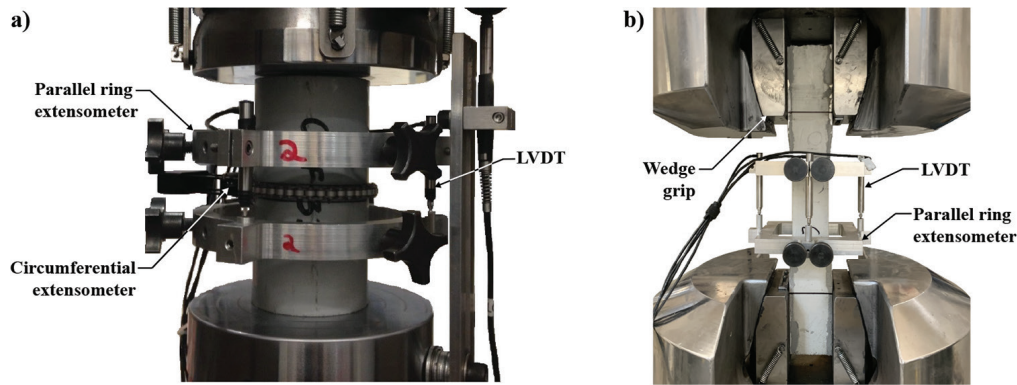


Fig. 1—(a) Compression test setup; and (b) direct tension test setup.

to elevated temperatures for approximately 48 hours, as is commonly done in precast plants in the northern United States, and specimens made of material U-J1b were covered and cured at outdoor ambient temperatures.

Compression testing

The compression test specimens were cast into cylindrical plastic molds having a diameter of 76.2 mm (3 in.) and a height of 152.4 mm (6 in.). The cylinder molds were filled vertically with a single lift of fresh UHPC. External vibration was subsequently applied for a brief period of 10 to 20 seconds using a concrete vibration table to help release entrapped air. The specimens were then covered and allowed to cure for 24 to 48 hours before they were demolded.

Compressive strength, modulus of elasticity, and Poisson's ratio tests were carried out on the UHPC cylinders according to ASTM C1856³⁶; ASTM C1856 provides modifications to ASTM C39²³ for UHPC compression testing, and modifications to ASTM C469²⁴ for UHPC elastic modulus and Poisson's ratio testing. Prior to testing, the specimen ends were ground flat and parallel using a fixed-end grinder. A minimum height-diameter ratio of 1.9 was maintained for all cylinders. Figure 1(a) shows the compression test setup prior to loading. The tests were completed under actuator displacement control corresponding to a load rate of 1.0 ± 0.05 MPa/s (145 ± 7 psi/s). The uniaxial strain was measured using three linear variable differential transformers (LVDTs) attached to a pair of parallel rings mounted on the cylinder over a gauge length of 76.2 mm (3 in.). The circumferential strain was captured using a chain-type extensometer mounted at midheight of the cylinder, as shown in Fig. 1(a). The chain-type extensometer measures the expansion of the cylinder's circumference during compression loading and is different than the traditional extensometer described in ASTM C469, which measures the change in the cylinder's diameter using two diametrically opposite points.

Direct tension testing

The tension test specimens were molded using prismatic steel molds having a length of 431.8 mm (17 in.) and cross-sectional dimensions of 50.8 x 50.8 mm (2 x 2 in.). Specimens were cast horizontally. Fresh UHPC was placed into the first one-quarter-length of the prism mold from one end and allowed to flow towards the other end. External vibration was subsequently applied for a brief period of 10

to 20 seconds using a concrete vibration table to help release entrapped air. The specimens were then covered with a plastic sheet and allowed to cure for 24 to 48 hours before being demolded and stored.

The tension tests were conducted according to AASTHO T 397 standard method of test.⁵⁰ This method allows the direct capture of the tensile load and associated strain applied over a known cross section and gauge length during a fixed-end, uniaxial displacement controlled test. Prior to testing, tapered aluminum plates were attached with a thin layer of epoxy on two parallel sides of each end of the specimen. The strain was captured over a gauge length of 101.6 mm (4 in.) using a parallel ring extensometer containing four LVDTs installed on each face of the specimen. Figure 1(b) shows the tension specimen in the test frame under load. Specimens were gripped at both ends using steel wedge grips and were subjected to a constant actuator displacement rate of 0.00254 mm/s (0.0001 in./s) until strain localization occurred. The displacement rate was then increased to 0.0254 mm/s (0.001 in./s) until a minimum strain value of 0.015 was achieved.

COMPRESSION BEHAVIOR

The general characteristics of UHPC's compressive stress-strain behavior can be observed in Fig. 2; a conventional concrete with a compressive strength of 41 MPa (6 ksi) is shown for comparison purposes. Compared to conventional concretes, UHPC-class materials are characterized by relatively high compressive strengths (greater than 124 MPa [18 ksi]), high stiffness (approximately 1.5 to 2 times greater than conventional concretes), relatively linear pre-peak behavior, and some reserve post-peak capacity. These characteristics are generally a byproduct of UHPC's densely packed, high-strength matrix, which is reinforced with discontinuous high-strength steel fibers that bridge the microcracking that forms during compression loading.

UHPC's stress-strain response in compression is characterized by an initial linearly elastic ascending branch with a slope corresponding to the modulus of elasticity, E . The ascending branch begins to soften beyond approximately $0.5f'_c$, likely due to formation of internal microcracks, as is the case with cementitious materials subjected to uniaxial compressive loads.^{50,51} The elastic modulus and the linearity of the stress-strain curve varies with compressive strength (or maturity), as shown in Fig. 2(b). That is, the higher the

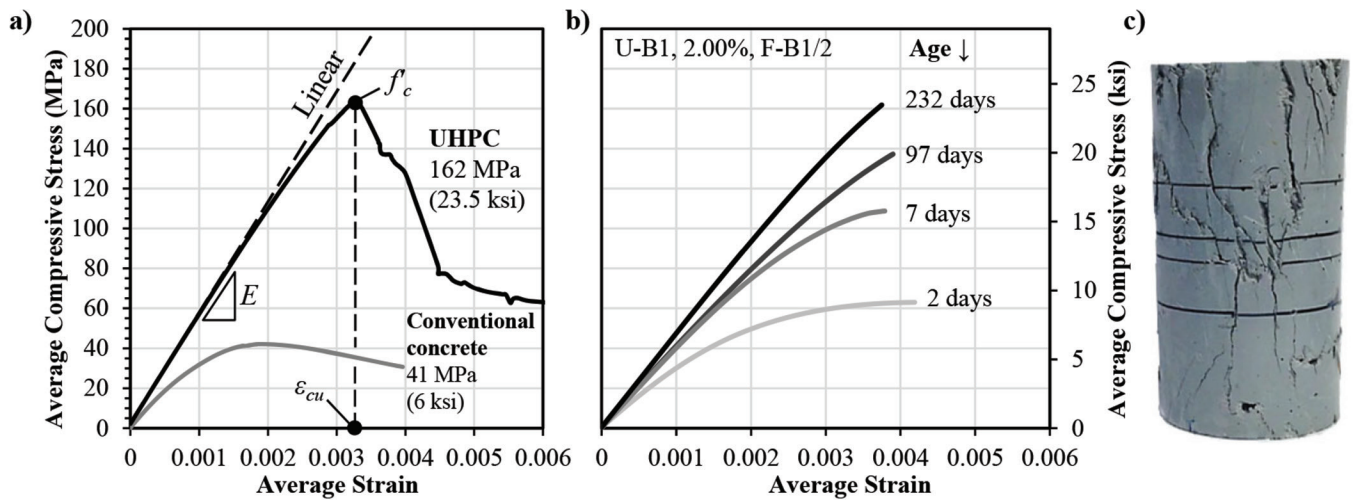


Fig. 2—(a) Experimental compressive response of UHPC and conventional concrete; (b) pre-peak compressive response of UHPC at different ages; and (c) crack pattern of UHPC cylinder at end of compression test.

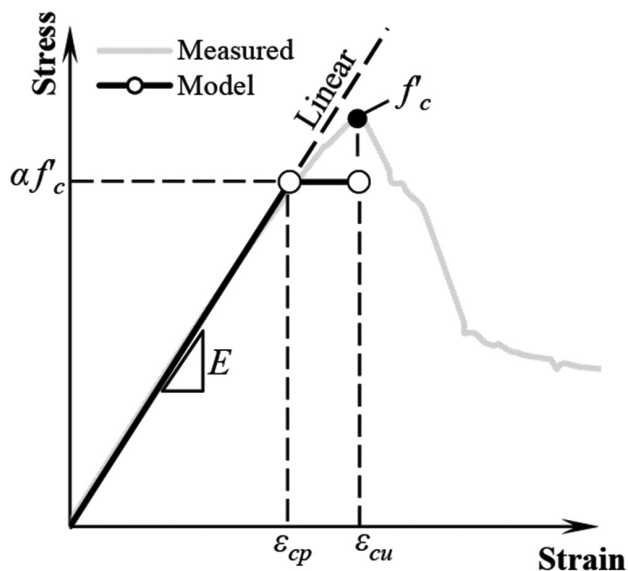


Fig. 3—Proposed compressive stress-strain model for UHPC design.

compressive strength, the more linear the stress-strain curve tends to remain prior to reaching peak stress (f_c'); this observation has been noted by previous research.^{13,52,53} The strength gain properties of UHPC-class materials are affected by the same variables as conventional concrete (for example, time, temperature, humidity, and use of admixtures^{8,17}) and can be designed to gain strength rapidly or exhibit long dwell times. The compressive strain at peak stress, ϵ_{cu} , is typically between 0.003 and 0.005 for most UHPC mixtures, and has some dependency on f_c' , as will be shown herein. UHPC-class materials have some reserve post-peak compressive strength capacity due to the inherent confinement provided by the high volume of the steel microfiber reinforcement. The cracking pattern of a UHPC compression cylinder after testing is shown in Fig. 2(c).

Compression design model

The proposed compression design model for UHPC is presented in Fig. 3 and superimposed atop a measured

compressive stress-strain curve for reference. The constitutive model is meant to capture the main characteristics of the UHPC's compressive behavior and be easily implemented by the engineering design community. Previous research on conventional concrete has shown that calculations using compression design models based solely on uniaxial compression testing can provide fairly accurate predictions of experimental beam test results.⁵³

The compression design model requires four input parameters and has two distinct branches: 1) a linear-elastic ascending branch; and 2) a perfectly plastic branch. The linear-elastic ascending branch is exclusively defined by the elastic modulus, E , which could be determined experimentally or estimated by an empirical expression. The transition from the linear-elastic branch to the plastic branch occurs once a reduced compressive strength is reached. The reduced strength is defined by multiplying the compressive strength, f_c' , by a reduction factor, α . Similar to conventional concrete design, f_c' would be specified or determined experimentally. The strain at this transition point, ϵ_{cp} , is determined using Hooke's law and the reduced compressive strength, $\alpha f_c'$. The plastic branch of the model terminates at the ultimate compressive design strain, denoted by ϵ_{cu} . Herein, it is proposed that ϵ_{cu} corresponds to the strain at peak compressive stress. As such, ϵ_{cu} would have a small range of acceptable values, which would be based on compression testing.

Compression results and typical design parameters

This section discusses the experimental results and proposes values for typical design parameters. The results are presented such that a constitutive compression response of UHPC can be proposed for a range of different UHPC-class products.

Elastic modulus—The elastic modulus of UHPC can be determined either by the experimental testing of a specified product, or, in absence of measured data, by a calibrated empirical relationship; the latter would be used predominantly in practice for design calculations when the full suite of mechanical properties for the UHPC that will be used is

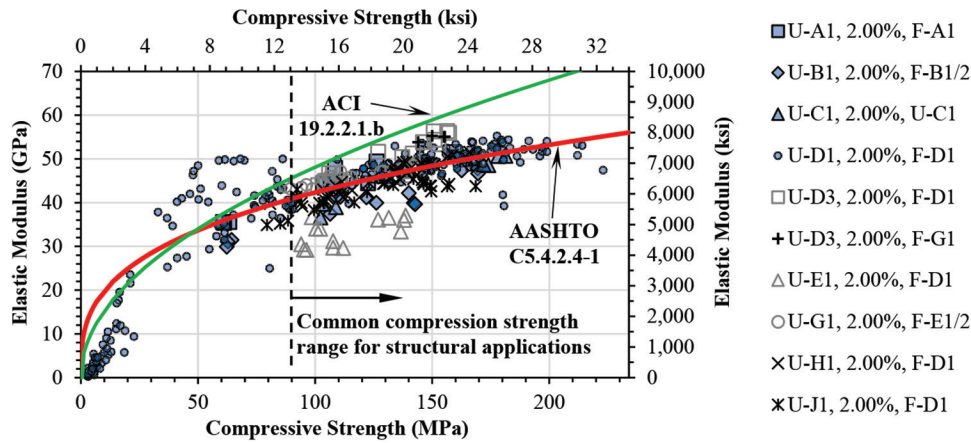


Fig. 4—Relationship between compressive strength and elastic modulus.

unknown. For conventional concretes, this relationship is traditionally calculated using an expression that is a root function of f'_c .^{22,55}

The elastic modulus results of 492 individual specimens made of 10 UHPC product-fiber product combinations are presented in Fig. 4 as a function of the measured compressive strength. To investigate the applicability of existing relationships between E and f'_c for UHPC, the elastic modulus equations prescribed in American Concrete Institute (ACI) 318 (Eq. (19.2.2.1.b))⁵⁵ and AASHTO LRFD (Eq. (C5.4.2.4-1))²² for normalweight concrete are superimposed atop of the experimental data, as shown in Fig. 4. The ACI equation, $E = 4700\sqrt{f'_c}$ (MPa) or $E = 57,000\sqrt{f'_c}$ (psi), overestimates the elastic modulus of UHPC for most of the data points obtained in this study (Fig. 4). The AASHTO LRFD equation, on the other hand, resulted in a good fit of the overall relationship between E and f'_c and is described in Eq. (1). This equation is proposed herein for use with UHPC materials because it resulted in a good approximation of the modulus of elasticity within the practical range of compressive strength values, between 127 and 200 MPa (14 and 29 ksi). This observation is revealed in Fig. 4 with the predicted $E - f'_c$ trend falling within the middle region of the experimental scatter.

$$E = 9100 f'_c{}^{0.33} \text{ (MPa)} \quad (1)$$

$$E = 2500 f'_c{}^{0.33} \text{ (ksi)}$$

It should be noted that the elastic modulus equations for conventional concretes in both ACI 318 and AASHTO LRFD included a density correction factor. The proposed equation for UHPC is independent of the density because the density variation of UHPC materials, between 2300 and 2800 kg/m³ (144 and 175 lb/ft³),^{28,29} is small compared to the density variation of conventional concrete, between 1400 and 2563 kg/m³ (90 and 160 lb/ft³).⁵⁵ In this study, the densities of the investigated materials were similar, with the average densities of all tested UHPC products ranging between 2371 and 2514 kg/m³ (148 and 157 lb/ft³).

Linearity of ascending branch—The proposed compression design model employs a linear-elastic ascending branch, as shown in Fig. 3. As such, it is important to discuss how this assumption aligns with the findings of the experimental program. Linearity was assessed for five UHPC

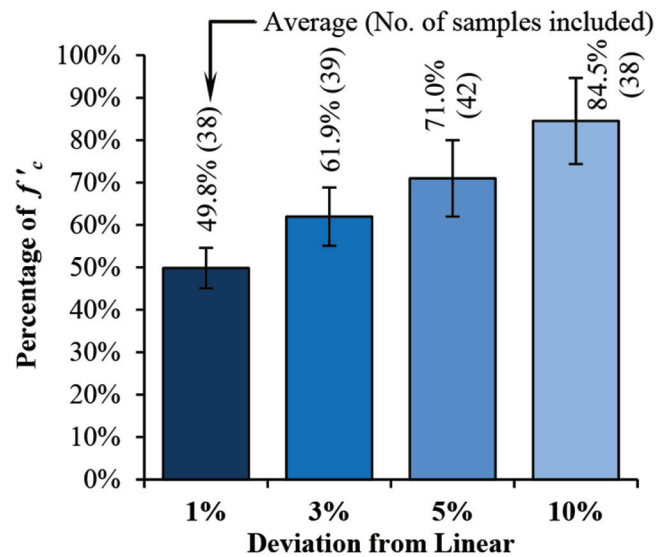


Fig. 5—Assessment of compressive stress-strain linearity; error bar represented \pm standard deviation.

product-fiber product combinations using the analytical methods described by Graybeal and Stone⁵³ and for samples exhibiting a compressive strength beyond 96 MPa (14 ksi). The results from this analysis are presented in Fig. 5. The horizontal axis of this plot depicts four different percentages, which represent the strain deviation from the linear response. The vertical axis represents the percentage of f'_c at which a given deviation from linearity occurs. That is, for example, a 5% deviation from linear stress-strain behavior occurs at a stress of $0.71f'_c$. This plot demonstrates that the compressive response of UHPC-class materials is highly linear (less than 10% deviation), even when 70 to 84.5% of f'_c is reached. As such, the compressive constitutive model's linear elastic ascending branch is a reasonable representation of the compressive behavior up to a strength of approximately $0.85f'_c$, and thus, a reduction factor, α , of 0.85 may be used to approximate of the linearly limit in design (Fig. 3).

Strain at peak compressive stress—The relationship between UHPC's compressive strength and axial strain at peak compressive stress is presented in Fig. 6 and is based on 401 data points and 10 UHPC product-fiber product combinations. The plot also depicts the average strain for

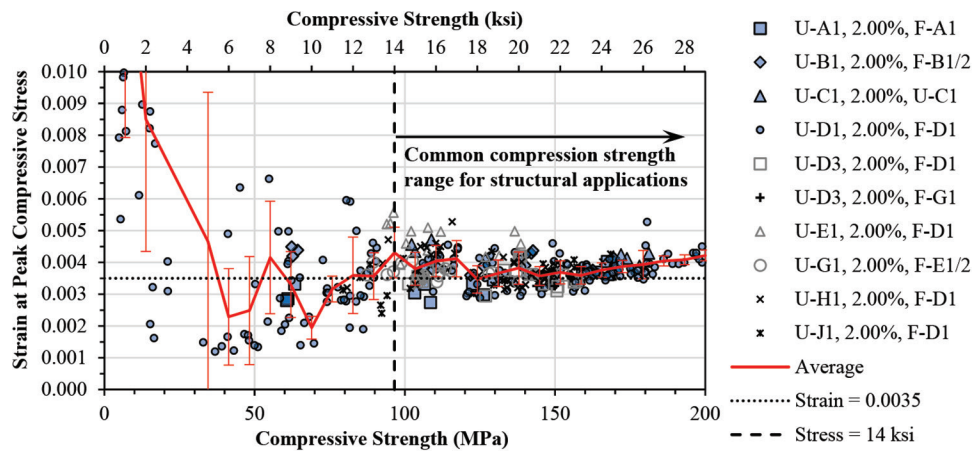


Fig. 6—Relationship between compressive strength and strain at peak compressive stress.

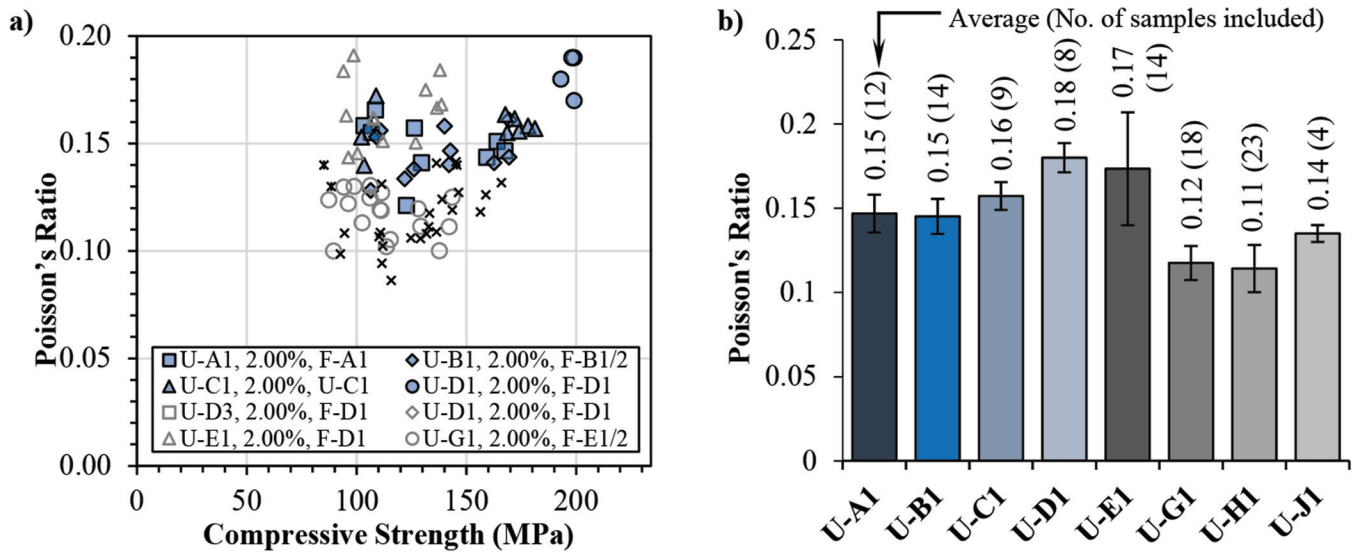


Fig. 7—Poisson's ratio of UHPC: (a) relationship between compressive strength and Poisson's ratio; and (b) average Poisson's ratio for UHPCs tested (error bars represent \pm standard deviation).

given compressive stress, and the error bars represent plus-or-minus one standard deviation. The strain at peak compressive stress varies significantly prior to a compressive strength of approximately 96 MPa (14 ksi). After which, the general response of UHPCs is more consistent, with 95.8% of the strain at peak stress values falling between 0.003 and 0.005 at an average of 0.0038, with a standard deviation of 0.00047. Based on these findings, it is recommended that ϵ_{cu} be taken between 0.003 and 0.005 in design of UHPC structural components. In lieu of experimental testing, a value 0.0035 can be taken for ϵ_{cu} for use in the design model of Fig. 3. This value is recommended because it falls below the average value of ϵ_{cu} for the majority of tested specimens, as shown in Fig. 6.

Poisson's ratio—The results for the Poisson's ratio, ν , are shown in Fig. 7(a) based on 102 data points included and eight UHPC product-fiber product combinations. The relationship between UHPC's compressive strength and Poisson's ratio is shown in Fig. 7(a), and the average Poisson's ratio values for specific UHPCs are shown in Fig. 7(b). The experimental data does not indicate a correlation between f'_c and ν , with approximately 98% of the Poisson's ratio

values falling between 0.1 and 0.2. Moreover, the Poisson's ratio for a given UHPC is generally consistent, as shown in Fig. 7(b). The average $\bar{\nu}$ for all data points is equal to 0.14 with a standard deviation of 0.029. Based on these findings, it is reasonable to assume that ν can be taken between 0.1 and 0.2 for design purposes. Herein, it is proposed that the design value of ν may be taken as 0.15 in lieu of physical testing. This value is chosen as it is close to the average value and falls at midrange of the experimental data.

TENSION BEHAVIOR

The tensile response of UHPC-class materials is a noteworthy feature of the material's mechanical behavior and is characterized by a significant strain capacity, post-cracking sustained resistance, and multiple tight and closely spaced discrete cracks. An example of a uniaxial stress-strain response of a UHPC specimen subjected to tensile loading is illustrated in Fig. 8. To visualize the fracture process, the strain field during the test was collected using a digital image correlation (DIC) technique over a target area of 50.8 x 101.6 mm (2 x 4 in.) at midlength of the specimen, as shown in Fig. 8(a). The tensile stress-strain

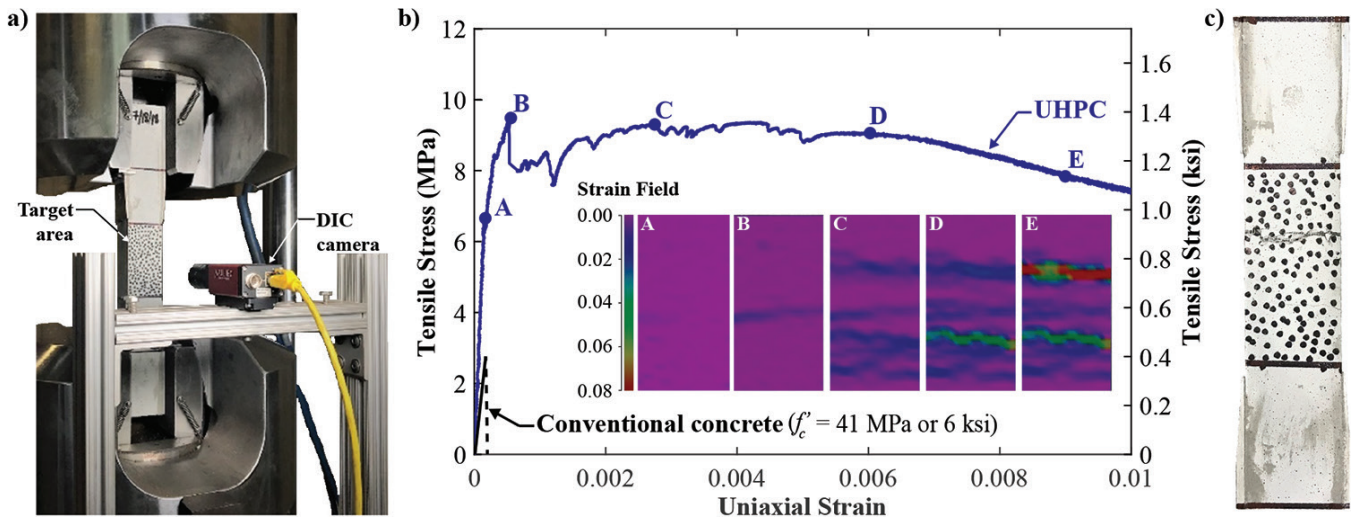


Fig. 8—(a) Tension test setup using DIC technique; (b) tensile stress-strain response and strain field of UHPC as compared to conventional concrete; and (c) crack pattern at end of UHPC tension test.

response, shown in Fig. 8(b), is characterized by an initial linearly elastic behavior with a slope corresponding to the modulus of elasticity, E . At onset of cracking (point A), a gradual loss of stiffness starts to occur until the effective cracking strength, $f_{t,cr}$, is reached at point B, where a discrete crack is developed over the full cross-sectional area of the specimen. As the material is strained beyond its cracking limit, fibers compensate for the lost tensile resistance of the matrix, leading to the formation of new fine cracks without significant loss in capacity (point C). This behavior characterizes UHPC materials and would not occur in conventional concrete or strain-softening, fiber-reinforced cementitious composites in which the occurrence of a crack is followed by a decrease in the load-carrying capacity. The multiple cracking (strain-hardening) phase continues until the fibers' ability to maintain the applied loads is exhausted, and the fibers start to pull out of the cementitious matrix at point D. The strain at crack localization is defined as the ultimate strain capacity of the material, $\epsilon_{t,loc}$, after which the deformation accumulates into a single crack and the tensile resistance starts to continuously decline. The response after crack localization, such as at point E, is more appropriately described as a function of crack opening rather than strain. The photograph of the test specimen shown in Fig. 8(c) demonstrates that after localization, a single, wide crack is often visible while other cracks have closed as the fibers bridging those cracks elastically unload.

Characteristic behavior and tension design models

The specific tensile response of the UHPC class of materials is not unique and depends on a variety of changing parameters, including matrix formulation, fiber amount, type, geometry, and orientation, as well as concrete maturity. Figure 9 shows examples of tensile stress-strain responses with strain-hardening characteristics captured as part of this study. Two types of characteristic behaviors can be identified. The first type designates materials exhibiting a stress plateau where the post-cracking stress remains

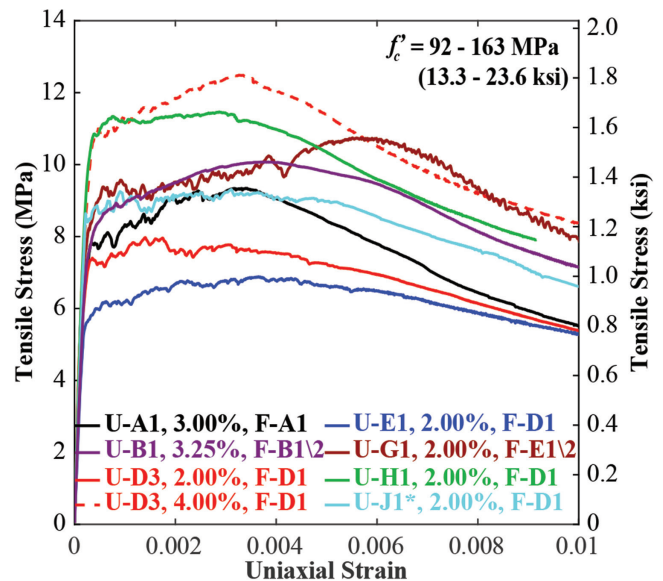


Fig. 9—Examples of tensile average stress-strain trends of eight UHPCs.

approximately equal to the effective cracking strength, $f_{t,cr}$, until strain localization occurs, as shown in Fig. 10(a). This type of response can be idealized by an elastic-plastic stress-strain model, as shown in Fig. 10(b). The second characteristic behavior corresponds to materials where the post-cracking stress continuously increases to an ultimate value occurring at the crack localization strain, $\epsilon_{t,loc}$, as shown in Fig. 10(a). This behavior can be idealized by the bilinear stress-strain model shown in Fig. 10(c). In both cases, the characteristic stress-strain design models mimic the general behavior of the tensile response and apply a reduction factor, γ , on the tensile resistance. The post-localization capacity of the material—that is, the descending branch of the response where the strain is greater than the crack localization strain, $\epsilon_{t,loc}$, is not accounted for in the models because the response is a function of crack opening and, therefore, it cannot be used in a strain-based design approach.

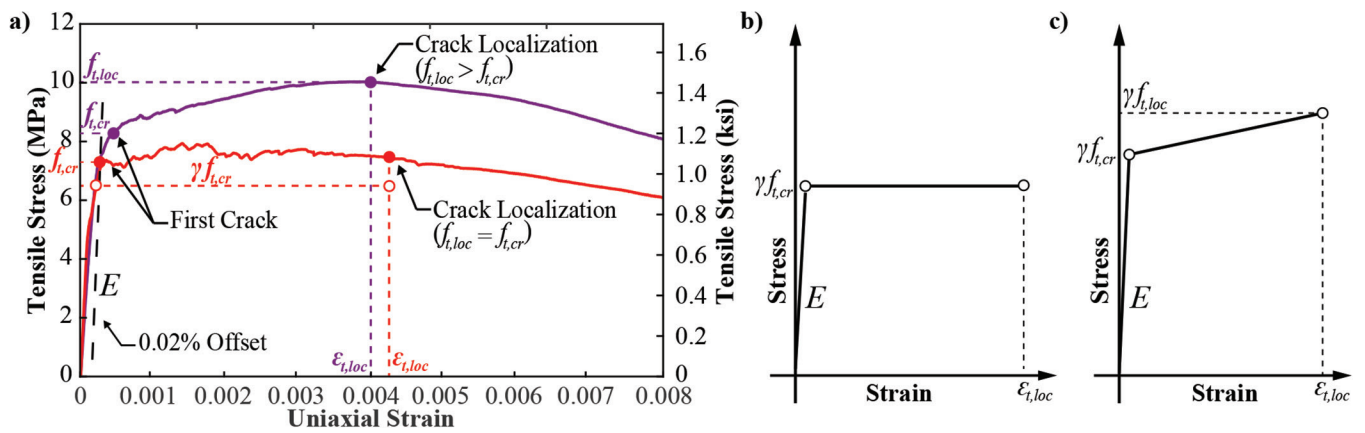


Fig. 10—(a) Examples of characteristic tensile stress-strain trends of UHPC-class materials; and idealized tensile stress-strain models for: (b) strain hardening with stress plateau; and (c) strain hardening with continuous increase in post-cracking stress.

The material models of Fig. 10 require the experimental determination of the elastic modulus, E , the first cracking stress, $f_{t,cr}$, and the strain localization stress, $f_{t,loc}$, and strain, $\epsilon_{t,loc}$. The tension elastic modulus value is generally equal to the elastic modulus obtained from a compression test and can be verified by calculating the slope of the tension stress-strain response at low levels of stress. The effective cracking stress can be visually identified from the stress-strain data—for example, the stress at the end of the elastic phase before a clear discontinuity is manifested by an abrupt drop in stress (point B in Fig. 8(b)). However, visually selecting the first cracking point is subject to user error and bias, and thus the offset method developed elsewhere and engaged by AASHTO T 397 was used to objectively determine the first cracking stress of all UHPC-class materials.^{13,50} The effective cracking stress, $f_{t,cr}$, is defined as the stress at the intercept of a line with a slope equal to the elastic modulus and a strain offset of 0.02 percent, as shown in Fig. 10(a). The localization stress, $f_{t,loc}$, and strain, $\epsilon_{t,loc}$, can be visually determined as the first point in the stress-strain trend, where the stress is continuously decreasing with increasing strain.

Tension response results

The experimental average of the tensile parameters of the UHPC-class materials tested in this study are listed in Table 1 (Table A-4 of Appendix III lists the results in the imperial system of units). The table details the results of the UHPC product-fiber product combinations that resulted in an effective cracking strength ($f_{t,cr}$) value greater than 5 MPa (0.73 ksi) sustained up to a minimum localization strain ($\epsilon_{t,loc}$) value of 0.0025. These minimum threshold values imposed on the key tensile parameters are recommended for structural components, as the thresholds establish a level of mechanical ductility and crack control characteristics that clearly distinguish UHPC-class materials from other fiber-reinforced cementitious composites. In addition, the idealized response is represented with the bilinear design model of Fig. 10(c) when the average localization stress is 20% greater than the average cracking stress ($\bar{f}_{t,loc} \geq 1.2\bar{f}_{t,cr}$). This limit is proposed to conservatively distinguish the two

types of tension behaviors and avoid the overestimation of the tensile stresses during design.

Effect of concrete maturity—The tensile strength gain with respect to concrete maturity is evaluated by performing a series of direct tension tests at various points in time during the curing process. Because the tests were not performed at a specific time for all mixtures, and given that the products contained various amounts of accelerating admixtures, the maturity of the tensile parameters is discussed with respect to the compressive strength. Figure 11(a) shows the average stress-strain trends of a subset of the results listed in Table 1 at various values of compressive strengths. The results indicate a strong correlation between the compressive and tensile strength gains with the tension strength increasing with the increase of compressive strength. For instance, the first cracking stress of U-H1 increased by 19.6% and 28.3% when the compressive strength increased from 100 to 130 MPa (14.5 to 18.8 ksi) and 143 MPa (20.8 ksi), respectively. This behavior is important when evaluating the in-place tensile properties of UHPC during construction, particularly for prestressed components at the time of strand detensioning. In contrast, a clear relationship between the localization stress and strain values and the compressive strength could not be definitively established from the limited number of relevant data points.

Effect of fiber content—Fibers crossing a crack plane compensate for the lost tensile resistance of the cementitious matrix by generating clamping forces that bridge the crack and arrest its propagation. When the amount of fibers in the matrix is increased, more fibers cross the crack interface resulting in an increase in the tensile capacity of the material. The average experimental results of Fig. 11(b) demonstrate this behavior, where adding more fibers to the same UHPC product improved the overall tension performance by increasing the cracking and ultimate stresses of the composite. For example, the cracking stress of U-D3 increased by 35.0% and 48.4% when the fiber volume was increased from 2.00% to 3.00% and 4.00%, respectively. Similar behavior was observed for all tested UHPC products listed in Table 1. In addition to the increase in the tensile capacity, adding fibers increased the post-cracking capacity of the composite, which changed the response from strain

Table 1—Key tension design parameters results for UHPC-class materials

UHPC ID	Fiber ID	v_f , %	\bar{f}_c' , MPa	No. of tests	$\bar{f}_{t,cr}^*$, MPa	$\bar{f}_{t,loc}^*$, MPa	$\bar{\epsilon}_{t,loc}^*$	Design model
U-A1	F-A1	2.00	111.7	5	4.78 [5.8%]	6.42 [12.0%]	0.0035 [26.7%]	Bilinear hardening
U-A1	F-A1	3.00	95.8	2	7.39 [1.8%]	9.76 [13.3%]	0.0028 [12.9%]	Bilinear hardening
U-A1	F-A1	3.00	104.8	4	6.84 [10.9%]	9.22 [8.7%]	0.0032 [13.9%]	Bilinear hardening
U-A1	F-A1	3.00	147.5	4	7.76 [6.5%]	9.48 [10%]	0.0029 [25.4%]	Bilinear hardening
U-B1	F-A1/2	2.00	153.1	1	7.56	8.32	0.0036	Elastic-plastic
U-B1	F-A1/2	3.25	101.4	3	8.2 [5.8%]	10.1 [5.7%]	0.0039 [10.6%]	Bilinear hardening
U-D1	F-D1	2.00	170.3	6	9.51 [13.4%]	10.48 [9.4%]	0.0055 [18.8%]	Elastic-plastic
U-D3	F-D1	2.00	93.8	4	7.05 [6.1%]	7.76 [6.4%]	0.0039 [40.5%]	Elastic-plastic
U-D3	F-D1	2.00	128.2	4	7.33 [6.0%]	7.90 [6.5%]	0.0038 [45.4%]	Elastic-plastic
U-D3	F-D1	2.00	154.9	3	7.28 [6.0%]	8.71 [3.8%]	0.0054 [23.8%]	Elastic-plastic
U-D3	F-G1	2.00	151.1	4	7.19 [7.5%]	8.68 [3.3%]	0.0066 [5.2%]	Bilinear hardening
U-D3	F-D1	2.50	96.5	1	8.35	9.12	0.0045	Elastic-plastic
U-D3	F-D1	3.00	84.8	4	8.26 [21.6%]	9.45 [20.2%]	0.0027 [17.6%]	Elastic-plastic
U-D3	F-D1	3.00	91.0	6	7.61 [4.3%]	8.16 [5.6%]	0.0030 [23.7%]	Elastic-plastic
U-D3	F-D1	3.00	122.0	2	9.89 [4.4%]	11.67 [11.1%]	0.0043 [18.6%]	Elastic-plastic
U-D3	F-D1	3.00	125.5	5	8.4 [6.4%]	9.36 [3.6%]	0.0046 [15.8%]	Elastic-plastic
U-D3	F-D1	4.00	100.0	3	10.5 [6.5%]	12.47 [7.1%]	0.0029 [24.5%]	Elastic-plastic
U-D3	F-D1	4.00	124.1	2	10.88 [5.4%]	12.53 [1.1%]	0.0033 [7.4%]	Elastic-plastic
U-E1	F-D1	2.00	91.7	5	5.84 [17.6%]	6.96 [15.9%]	0.0040 [26.6%]	Elastic-plastic
U-E1	F-D1	2.00	118.6	2	7.14 [12.8%]	8.76 [14.5%]	0.0051 [34.1%]	Bilinear hardening
U-E1	F-D1	3.25	100.7	2	9.69 [5.4%]	11.76 [8.1%]	0.0039 [52.4%]	Bilinear hardening
U-E1	F-D1	3.25	120.0	2	7.68 [3.9%]	10.35 [7.4%]	0.0038 [2.1%]	Bilinear hardening
U-G1	F-E1/2	2.00	100.0	3	6.71 [11.3%]	8.2 [9.5%]	0.0064 [20.4%]	Bilinear hardening
U-G1	F-E1/2	2.00	129.6	4	8.03 [14.6%]	10.88 [5.3%]	0.0058 [20.5%]	Bilinear hardening
U-G1	F-E1/2	2.00	143.4	3	8.61 [4.9%]	10.81 [7.3%]	0.0059 [7.4%]	Bilinear hardening
U-H1	F-D1	2.00	112.4	4	8.41 [11.4%]	10 [6.1%]	0.0033 [15.2%]	Elastic-plastic
U-H1	F-D1	2.00	162.7	5	10.81 [5.6%]	11.3 [4.8] %	0.0039 [16.9%]	Elastic-plastic
U-H2b	F-D1	2.00	137.2	3	10.5 [8.9%]	11.29 [7%]	0.0037 [4.4%]	Elastic-plastic
U-H2b	F-D1	2.00	140.0	6	10.82 [6.0%]	10.72 [6.7%]	0.0032 [39.8%]	Elastic-plastic
U-J1b	F-D1	2.00	152.4	4	8.90 [12.0%]	9.25 [14.5%]	0.0044 [21.8%]	Elastic-plastic
U-J1b	F-D1	2.00	157.9	3	7.91 [4.6%]	8.61 [9.0%]	0.0052 [9.3%]	Elastic-plastic

*Values in brackets represent the coefficient of variation, taken as the ratio of standard deviation to the mean value.

Note: 1 MPa = 0.145 ksi.

hardening with stress plateau (Fig. 10(b)) to bilinear hardening (Fig. 10(c)), as shown in Table 1 for UHPC products U-B1 and U-E1. Finally, a general trend of decreasing values of the localization strain with the addition of fibers and the increase in tensile capacity was observed and clearly detected for UHPC products U-E1 and U-D3 (Fig. 11(b) and Table 1).

Effect of fiber type—The effectiveness of the fibers in controlling cracks and improving the tensile resistance depends on the fiber chemical composition and its mechanical and geometrical properties, as well as the chemical composition of the matrix. These factors establish the fiber-matrix bond behavior that results in the frictional fiber pullout behavior necessary to increase the energy dissipation of the

composite after cracking and establish the tensile ductility characteristic of UHPC-class materials.⁷ Figure 11(c) shows the average stress-strain trends of two UHPC products (U-D and U-H) mixed with four fiber products (F-D1, F-G1, F-F1, and F-P1). To demonstrate the effect of the matrix composition, UHPC products U-D1, U-D3, and U-H1 were dosed with similar volume fractions ($v_f = 2.00\%$) of fiber product F-D1 and resulted in dissimilar stress-strain response with each combination. For instance, the cracking stress was 7.28, 9.51, and 10.81 MPa (1.1, 1.4, and 1.57 ksi), when F-D1 was mixed with U-D1, U-D3, and U-H1, respectively. Moreover, UHPC product U-H1 localized at a lower strain value ($\epsilon_{t,loc} = 0.0039$) than products U-D1 ($\epsilon_{t,loc} = 0.0055$) and U-D3 ($\epsilon_{t,loc} = 0.0054$). The increase in stress capacity

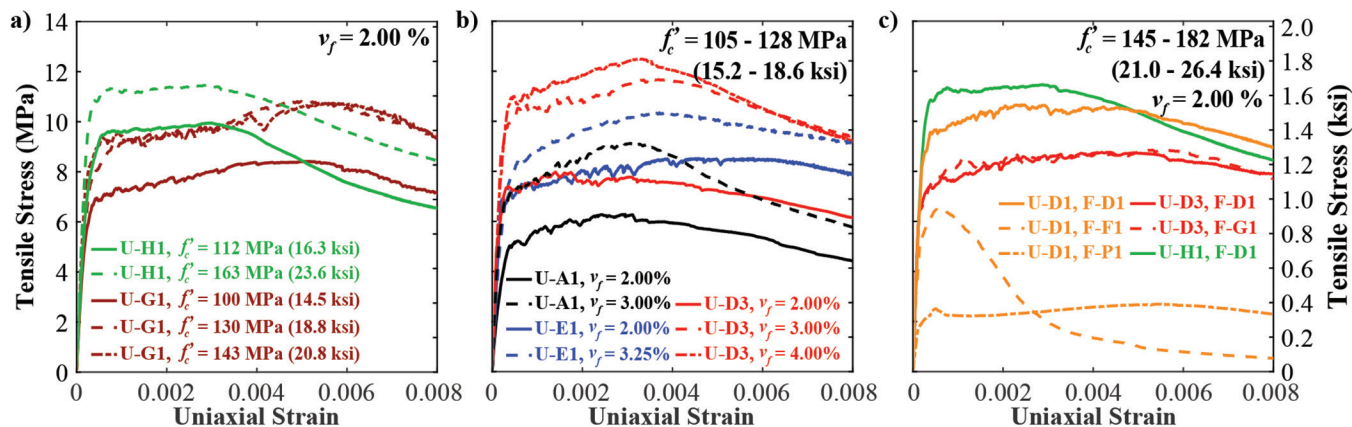


Fig. 11—Tensile stress-strain trends for UHPC-class materials showing effect of: (a) compressive strength; (b) fiber content; and (c) fiber product.

can be attributed to changes in the chemical composition of the matrix, resulting in improved fiber-matrix bond strength without exceeding the ultimate tensile strength of the fibers. The effect of the ultimate tensile strength of the fibers and fiber geometry is investigated by dosing UHPC product U-D1 with similar volume fractions ($v_f = 2.00\%$) of fiber product F-D1 and F-F1. These fiber products reported tensile strengths of 2600 and 689 MPa (377 and 100 ksi), a length of 13 mm (0.51 in.), and cross-sectional areas of 0.031 and 0.18 mm² (0.000049 and 0.029 in.²), respectively. These differences in properties translate to 5.8 times fewer individual fibers for product F-F1 compared to F-D1 in the same mixture volume. Moreover, individual F-F1 fibers can carry 124.0 N (27.9 lb) of force before rupture compared to 80.6 N (18.1 lb) for F-D1. The resulting stress-strain trends, shown in Fig. 11(c), indicate that fiber product F-F1 did not provide adequate post-cracking capacity expected of UHPC materials, likely attributed to insufficient clamping forces at the vicinity of cracks. Similar behavior is also observed when UHPC product U-D1 is combined with fiber product F-P1, as shown in Fig. 11(c). Fiber product F-P1 is made of PVA and has an elastic modulus (28.9 GPa [4200 ksi]) significantly lower than steel, a tensile capacity of 1000 MPa (145 ksi), and a length of 12 mm (0.5 in.). Finally, fiber products with similar chemical, geometrical, and mechanical properties can result in similar stress-strain trends as is the case with fiber product U-D3 combined with fiber products F-H1 and F-G1, as shown in Fig. 11(c). More information on the effect of fiber type on the tensile behavior of UHPC can be found in Graybeal.¹²

Effect of fiber orientation—Fiber orientation in structural members has a significant effect on the tensile response of in-place UHPC. Fibers tend to preferentially align with the flow direction of fresh UHPC during casting, resulting in anisotropic tensile resistance between the flow and nonflow directions. Therefore, in places where tensile stress resistance is critical to the integrity of the structure, further investigation on the fiber orientation might be necessary. However, in many cases, specifying a casting method and construction practices that establish a fiber orientation similar to the one assumed in the design phase may be sufficient. The fiber orientation effect is demonstrated by, among

others,^{51,56,57} the work of Maya Duque and Graybeal.⁵⁸ This study investigated the tensile response of prismatic specimens extracted from a UHPC slab at orientation angles of 0, 45, and 90 degrees with respect to the flow direction. Compared to the mold-cast companion specimens made with the same UHPC and fiber content ($v_f = 2.00\%$), the average tensile strength decreased by 29.7% and 80.0% for extracted specimens at angles of 45 and 90 degrees with respect to the flow direction, respectively. However, the tensile strength increased by 12.9% for the specimens extracted parallel to the flow direction when compared to the companion specimens cast in prismatic molds. Although a portion of the decrease in stresses might be attributed to discontinuities in the extracted specimens causing stress concentrations and promoting early cracking, the results indicate a strong correlation between fiber orientation and tensile behavior that must be considered in the design and construction of components made with UHPC-class materials.

TYPICAL PROPERTIES, DESIGN MODELS, AND MINIMUM PERFORMANCE METRICS FOR STRUCTURAL-GRADE UHPC

Before incorporating a construction material into structural design, it is necessary to establish specific performance metrics that guarantee the anticipated behavior assumed during the design phase. For structural members made with UHPC-class materials, the authors relied on national and international experiences supported with the experimental data presented in this paper to make conservative recommendations for typical material properties and minimum threshold property values that are required to qualify a UHPC product for structural applications.

Proposed UHPC definition

In general, UHPC-class materials are portland cement composite materials composed of an optimized gradation of granular constituents, a water-cementitious materials ratio (w/cm) less than 0.28, and a high percentage of discontinuous internal steel fiber reinforcement, which ensures tensile strain-hardening behavior. The following mature age mechanical properties are required:

Table 2—Proposed test methods, typical mechanical properties, and threshold property values of UHPC-class materials for use in structural design

Property	Test method	Typical values	Minimum value
Young’s modulus E	ASTM C469 and ASTM C1856	45 to 65 GPa (6500 to 9400 ksi)	n/a*
Compressive strength f_c'	ASTM C39 and ASTM C1856	145 to 250 MPa (21.0 to 36.3 ksi)	124 MPa (18.0 ksi)
Ultimate compressive strain ϵ_{cu}	ASTM C469 and ASTM C1856	0.003 to 0.005	n/a*
Poisson’s ratio ν	ASTM C469 and ASTM C1856	0.1 to 0.2	n/a*
Effective cracking strength $f_{t,cr}$	AASHTO T 397 ^{†,‡}	6.2 to 12.4 MPa (0.90 to 1.80 ksi)	5.0 MPa (0.73 ksi)
Localization stress $f_{t,loc}$	AASHTO T 397 ^{†,§}	6.2 to 12.4 MPa (0.90 to 1.80 ksi)	$\geq f_{t,cr}$
Localization strain $\epsilon_{t,loc}$	AASHTO T 397 ^{†,§}	0.003 to 0.008	0.0025

*Indicates that there is no required minimum value for this particular property.

[†]Test method by uniaxial tension test method; obtains the stress-strain response of the tested specimen.

[‡]Determined using a 0.02% strain offset line with slope equal to the modulus of elasticity.

[§]Stress and strain of data point where the stress is continually decreasing with increasing strain.

- A minimum compressive strength, f_c' , of 124 MPa (18.0 ksi).
- A minimum effective cracking strength, $f_{t,cr}$, of 5.0 MPa (0.73 ksi).
- The ability to sustain the effective cracking strength, through a minimum localization strain, $\epsilon_{t,loc}$, of 0.0025.

Durability criteria will be described in future publications. These mechanical properties shall be determined according to specified test methods designated in the following section.

Proposed test methods and design models

The compression parameters—namely, the modulus of elasticity E , compressive strength f_c' , ultimate compression strain ϵ_{cu} , and Poisson’s ratio ν —shall be obtained from cylindrical specimens tested according to ASTM C39²³ and ASTM C469²⁴ with provisions specific to UHPC outlined in ASTM C1856.³⁶ For design, in lieu of experimental tests, the modulus of elasticity can be determined by the relationship of Eq. (1), as a function of the compressive strength, and the Poisson’s ratio may be taken as 0.15. The constitutive law of UHPC in compression shall be treated as linearly elastic until the stress reaches $\alpha f_c'$, where α is the reduction factor that can be taken as 0.85. Beyond this stress, the model sustains this compressive resistance until the strain at the material’s compressive strength is reached, ϵ_{cu} , as shown in Fig. 3. In lieu of physical tests, the ultimate strain, ϵ_{cu} , can be taken as the greater of $\epsilon_{cu} = \alpha f_c' / E$ and 0.0035.

The tension parameters—namely, the modulus of elasticity E , the effective cracking strength $f_{t,cr}$, the localization stress $f_{t,loc}$, and the localization strain $\epsilon_{t,loc}$ —shall be obtained from prismatic specimens tested in uniaxial tension according to AASHTO T 397.⁵⁰ This method results in uniaxial stress-strain responses of the tested specimens, allowing the identification of all the tension parameters. The effective cracking strength, $f_{t,cr}$, is taken as the intercept of a line having a slope equal to the elastic modulus and a strain offset of 0.02%, as shown in Fig. 10(a). The localization stress, $f_{t,loc}$, and strain, $\epsilon_{t,loc}$, are taken as the stress and strain of the data point

where the stress is consistently decreasing with increasing strain, without substantial recovery, as shown in Fig. 10(a). The localization point should not be taken at a point on the stress-strain curve where the stress is smaller than $f_{t,cr}$. The constitutive law for UHPC in tension shall be treated as an elastic-plastic model, shown in Fig. 10(b), for materials exhibiting a stress plateau, or a bilinear relationship, shown in Fig. 10(c), for material exhibiting a continuous increase in stress after cracking and when the localization stress, $f_{t,loc}$, is 20% greater than the effective cracking stress, $f_{t,cr}$. A reduction factor, γ , is applied to both the $f_{t,cr}$ and the $f_{t,loc}$ and can be taken as 0.85.

Typical parameters for use in structural design with UHPC

Table 2 presents a synopsis of the proposed material test methods for UHPC, typical mechanical properties, and the minimum threshold values to qualify a UHPC material for use in load-bearing components. The typical values presented in Table 2 can be used by owners and designers as indicators of the values expected from currently available UHPC materials.

CONCLUSIONS

This paper presents an experimental investigation of the compression and tension behaviors of commercially available ultra-high-performance concrete (UHPC) products. The data were then used to establish suitable strain-based mechanical design models for UHPC and to establish minimum performance metrics for the use of UHPC in structural applications. Based on these investigations, the following conclusions can be drawn:

- UHPC tensile and compressive behaviors can be quantitatively documented through the execution of uniaxial stress-strain testing methods, and parameters derived from these test results can be used to formulate stress-strain models that simulate the mechanical performance.

- The compression behavior of UHPC can be idealized by an elastic-plastic, stress-strain model for use in structural design. The model requires three material properties—namely, the modulus of elasticity, the compressive strength, and the strain at ultimate stress. These properties can be obtained from compression tests performed on cylindrical specimens according to ASTM C1856.³⁶ The mature compressive strength of UHPC used in structural applications is recommended to be at least 124 MPa (18 ksi), and the strength at the time of first structural loading is recommended to be at least 96 MPa (14 ksi). In lieu of experimental testing, the modulus of elasticity can be approximated through a proposed empirical relationship as a function of the compressive strength, and the ultimate strain can be taken as 0.0035.
- The results of compression testing indicate that the modulus of elasticity and the linearity of the stress-strain curve increase with increasing compressive strength and maturity of the material. The strain at ultimate compressive strength does not appear to significantly vary with compressive strength as 98.5% of the values fall between 0.003 and 0.005 when the compressive strength is above 96 MPa (14 ksi).
- The tension behavior can be idealized by an elastic-plastic or bilinear stress-strain relationship for use in structural design. The model requires four material property parameters obtained by executing a direct tension test on UHPC prismatic specimens—namely, the modulus of elasticity, the cracking stress, and the localization stress and strain. These properties can be obtained from uniaxial tension testing performed on prismatic specimens. For use in structural design, it is recommended that the effective cracking strength be at least 5 MPa (0.73 ksi) and the effective cracking strength must be sustained through a localization strain of at least 0.0025.
- There is a positive correlation between the increasing compressive strength of UHPC with time, and the concurrent increase in the tensile strength of the same material over the same time period.
- The tensile response of UHPC products depends on both the composition of the cementitious materials and the properties and type of the reinforcing fibers, as well as the relative quantity and orientation of the reinforcing fibers. Fibers that deliver a high-bond stress with the UHPC matrix, while able to pull out without rupturing when subjected to tensile loads, led to an increase in UHPC tensile capacities. An increase in the UHPC tensile strength was also observed with increased fiber amount and when the direction of tensile loading was aligned with the orientation of the fibers, which is affected by the flow direction during casting. Increasing the fiber amount appeared to decrease the strain capacity of the material.

AUTHOR BIOS

ACI member Rafic G. El-Helou is a Researcher with Genex Systems at the Turner-Fairbank Highway Research Center (TFHRC). He received his BE in civil engineering from the Lebanese American University, Beirut, Lebanon; his MS in civil engineering from Syracuse University, Syracuse, NY; and his PhD in civil engineering from Virginia Polytechnic Institute and

State University, Blacksburg, VA. His research interests include behavior and constitutive modeling of advanced civil engineering materials, experimental testing and modeling of concrete structures, and design methods.

ACI member Zachary B. Haber is a Research Structural Engineer with the Federal Highway Administration (FHWA) at TFHRC. He received his BS and MS in civil engineering from the University of Central Florida, Orlando, FL, and his PhD in civil engineering from the University of Nevada, Reno, NV. His research interests include large-scale testing, advanced materials in civil engineering, and bridge engineering.

ACI member Benjamin A. Graybeal is the Team Leader for bridge engineering research with FHWA at TFHRC. He received his BS and MS in civil engineering from Lehigh University, Bethlehem, PA, and his PhD from the University of Maryland, College Park, MD. He is the Chair of ACI Committee 239, Ultra-High-Performance Concrete. His research interests include bridge engineering, advanced infrastructure materials, and forensic structural engineering.

ACKNOWLEDGMENTS

The research presented in this paper was funded by FHWA. This support is gratefully acknowledged. The publication of this paper does not necessarily indicate approval or endorsement of the findings, opinions, conclusions, or recommendations either inferred or specifically expressed herein by FHWA or the United States Government. This research could not have been completed were it not for the dedicated support of the technical professionals associated with the FHWA Structural Concrete Research Program.

REFERENCES

1. De Larard, F., and Sedran, T., "Mixture-Proportioning of High-Performance Concrete," *Cement and Concrete Research*, V. 32, No. 11, 2002, pp. 1699-1704. doi: 10.1016/S0008-8846(02)00861-X
2. Li, V. C., "On Engineered Cementitious Composites (ECC)," *Journal of Advanced Concrete Technology*, V. 1, No. 3, 2003, pp. 215-230. doi: 10.3151/jact.1.215
3. Habel, K.; Viviani, M.; Denarié, E.; and Brühwiler, E., "Development of the Mechanical Properties of an Ultra-High Performance Fiber Reinforced Concrete (UHPRFC)," *Cement and Concrete Research*, V. 36, No. 7, 2006, pp. 1362-1370. doi: 10.1016/j.cemconres.2006.03.009
4. Graybeal, B., and Tanesi, J., "Durability of an Ultrahigh-Performance Concrete," *Journal of Materials in Civil Engineering*, ASCE, V. 19, No. 10, 2007, pp. 848-854. doi: 10.1061/(ASCE)0899-1561(2007)19:10(848)
5. Lepech, M. D., and Li, V. C., "Water Permeability of Engineered Cementitious Composites," *Cement and Concrete Composites*, V. 31, No. 10, 2009, pp. 744-753. doi: 10.1016/j.cemconcomp.2009.07.002
6. Magureanu, C.; Sosa, I.; Negrutiu, C.; and Heghes, B., "Mechanical Properties and Durability of Ultra-High-Performance Concrete," *ACI Materials Journal*, V. 109, No. 2, Mar.-Apr. 2012, pp. 177-184.
7. Wille, K., and Naaman, A. E., "Effect of Ultra-High-Performance Concrete on Pullout Behavior of High-Strength Brass-Coated Straight Steel Fibers," *ACI Materials Journal*, V. 110, No. 4, July-Aug. 2013, pp. 451-462.
8. Graybeal, B. A., "Material Property Characterization of Ultra-High Performance Concrete," *Report No. FHWA-HRT-06-103*, Federal Highway Administration, McLean, VA, 2006.
9. Wille, K.; Naaman, A. E.; and Parra-Montesinos, G. J., "Ultra-High Performance Concrete with Compressive Strength Exceeding 150 MPa (22 ksi): A Simpler Way," *ACI Materials Journal*, V. 108, No. 1, Jan.-Feb. 2011, pp. 46-54.
10. El-Helou, R. G., "Multiscale Computational Framework for Analysis and Design of Ultra-High Performance Concrete Structural Components and Systems," PhD dissertation, Virginia Polytechnic Institute and State University, Blacksburg, VA, 2016.
11. Wille, K.; Kim, D. J.; and Naaman, A. E., "Strain-Hardening UHP-FRC with Low Fiber Contents," *Materials and Structures*, V. 44, No. 3, 2011, pp. 583-598. doi: 10.1617/s11527-010-9650-4
12. Graybeal, B. A., "Tensile Mechanical Response of Ultra-High-Performance Concrete," *Advances in Civil Engineering Materials*, V. 4, No. 2, 2015, pp. 62-74.
13. Haber, Z.; De La Varga, I.; Graybeal, B.; Nakashoji, B.; and El-Helou, R., "Properties and Behavior of UHPC-Class Materials," *Report No. FHWA-HRT-18-036*, Federal Highway Administration, McLean, VA, 2018.
14. Kusumawardaningsih, Y.; Fehling, E.; Ismail, M.; and Aboubakr, A. A. M., "Tensile Strength Behavior of UHPC and UHPFRC," *Procedia Engineering*, V. 125, 2015, pp. 1081-1086. doi: 10.1016/j.proeng.2015.11.166
15. Kang, S.-T.; Lee, Y.; Park, Y.-D.; and Kim, J.-K., "Tensile Fracture Properties of an Ultra-High Performance Fiber Reinforced Concrete

(UHPC) with Steel Fiber,” *Composite Structures*, V. 92, No. 1, 2010, pp. 61-71. doi: 10.1016/j.compstruct.2009.06.012

16. Zhou, Z., and Qiao, P., “Tensile Behavior of Ultra-High-Performance Concrete: Analytical Model and Experimental Validation,” *Construction and Building Materials*, V. 201, 2019, pp. 842-851. doi: 10.1016/j.conbuildmat.2018.12.137

17. Russel, H., and Graybeal, B., “Ultra-High Performance Concrete: A State-of-the-Art Report for the Bridge Community,” *Report No. FHWA-HRT-13-060*, Federal Highway Administration, McLean, VA, 2013.

18. El-Helou, R., and Graybeal, B., “The Ultra Girder: A Design Concept for a 300-foot Single Span Prestressed Ultra High-Performance Concrete Bridge Girder,” *2nd International Interactive Symposium on Ultra-High Performance Concrete*, Albany, NY, 2019.

19. Sritharan, S., “Design of UHPC Structural Members: Lessons Learned and ASTM Test Requirements,” *Advances in Civil Engineering Materials, An ASTM Journal*, V. 4, No. 2, 2015, pp. 113-131. doi: 10.1520/ACEM20140042

20. Wipf, T. J.; Phares, B. M.; Sritharan, S.; Degen, E. B.; and Giesmann, T. M., “Design and Evaluation of a Single-Span Bridge Using Ultra-High Performance Concrete,” Iowa State University Institute for Transportation, Ames, IA, 2009.

21. Graybeal, B., “Design and Construction of Field-Cast UHPC Connections,” *TechNote No. FHWA-HRT-14-084*, Federal Highway Administration, McLean, VA, 2014.

22. AASHTO, “AASHTO LRFD Bridge Design Specifications, 9th Edition,” American Association of State Highway and Transportation Officials, Washington, DC, 2020.

23. ASTM C39/C39M-18, “Standard Test Method for Compressive Strength of Cylindrical Concrete Specimens,” ASTM International, West Conshohocken, PA, 2018.

24. ASTM C469/C469M-14, “Standard Test Method for Static Modulus of Elasticity and Poisson’s Ratio of Concrete in Compression,” ASTM International, West Conshohocken, PA, 2014.

25. AASHTO T 97, “Standard Method of Test for Flexural Strength of Concrete (Using Simple Beam with Third-Point Loading),” American Association of State Highway and Transportation Officials, Washington, DC, 2018.

26. ASTM C78/C78M-18, “Standard Test Method for Flexural Strength of Concrete (Using Simple Beam with Third-Point Loading),” ASTM International, West Conshohocken, PA, 2018.

27. NF P18-470, “Ultra-High Performance Fibre-Reinforced Concrete—Specifications, Performance, Production, and Conformity,” Association Française de Normalization (AFNOR - French Standard Institute), Paris, France, 2016.

28. NF P18-710, “National Addition to the Eurocode 2—Design of Concrete Structures: Specific Rules for Ultra-High Performance Fibre-Reinforced Concrete (UHPC),” Association Française de Normalisation (AFNOR - French Standard Institute), Paris, France, 2016.

29. SIA 2052, “Recommendation: Ultra-High Performance Fibre-Reinforced Cement-based Composites (UHPC) Construction Material, Dimensioning, and Application,” Swiss Federal Institute of Technology, Lausanne, Switzerland, 2016.

30. CSA S6-19, “Canadian Highway Bridge Design Code,” Canadian Standards Association, Toronto, ON, Canada, 2019.

31. CSA A23.1:19/CSA A23.2:19, “Concrete Materials and Methods of Concrete Construction/Test Methods and Standard Practices for Concrete,” Canadian Standards Association, Toronto, ON, Canada, 2019.

32. Lopez, J. A.; Serna, P.; and Navarro-Gregori, J., “Advances in the Development of the First UHPC Recommendations in Spain: Material Classification, Design and Characterization,” *AFGC-ACI-fib-RILEM International Symposium on Ultra-High-Performance Fibre-Reinforced Concrete*, Montpellier, France, 2017, pp. 565-574.

33. Schmidt, M.; Leutbecher, T.; Piotrowski, S.; and Wiens, U., “The German Guideline for Ultra-High-Performance Concrete,” *AFGC-ACI-fib-RILEM International Symposium on Ultra-High-Performance Fibre-Reinforced Concrete*, Montpellier, France, 2017, pp. 545-555.

34. JSCE, “Recommendations for Design and Construction of High-Performance Fiber Reinforced Cement Composites with Multiple Fine Cracks (HPFRCC),” Japan Society of Civil Engineers, Tokyo, Japan, 2008.

35. JSCE, “Recommendations for Design and Construction of Ultra High Strength Fiber Reinforced Concrete Structures (Draft),” Japan Society of Civil Engineers, Tokyo, Japan, 2006.

36. ASTM C1856/C1856M-17, “Standard Practice for Fabricating and Testing Specimens of Ultra-High Performance Concrete,” ASTM International, West Conshohocken, PA, 2017, 4 pp.

37. ASTM C496/C496M-17, “Standard Test Method for Splitting Tensile Strength of Cylindrical Concrete Specimens,” ASTM International, West Conshohocken, PA, 2017.

38. Park, S. H.; Kim, D. J.; Ryu, G. S.; and Koh, K. T., “Tensile Behavior of Ultra High Performance Hybrid Fiber Reinforced Concrete,” *Cement and Concrete Composites*, V. 34, No. 2, 2012, pp. 172-184. doi: 10.1016/j.cemconcomp.2011.09.009

39. Hassan, A. M. T.; Jones, S. W.; and Mahmud, G. H., “Experimental Test Methods to Determine the Uniaxial Tensile and Compressive Behaviour of Ultra High Performance Fibre Reinforced Concrete (UHPC),” *Construction and Building Materials*, V. 37, 2012, pp. 874-882. doi: 10.1016/j.conbuildmat.2012.04.030

40. Wille, K.; El-Tawil, S.; and Naaman, A. E., “Properties of Strain Hardening Ultra High Performance Fiber Reinforced Concrete (UHP-FRC) under Direct Tensile Loading,” *Cement and Concrete Composites*, V. 48, 2014, pp. 53-66. doi: 10.1016/j.cemconcomp.2013.12.015

41. Tran, N. T.; Tran, T. K.; and Kim, D. J., “High Rate Response of Ultra-High-Performance Fiber-Reinforced Concrete under Direct Tension,” *Cement and Concrete Research*, V. 69, 2015, pp. 72-87. doi: 10.1016/j.cemconres.2014.12.008

42. Pyo, S.; El-Tawil, S.; and Naaman, A. E., “Direct Tensile Behavior of Ultra High Performance Fiber Reinforced Concrete (UHP-FRC) at High Strain Rates,” *Cement and Concrete Research*, V. 88, 2016, pp. 144-156. doi: 10.1016/j.cemconres.2016.07.003

43. Choi, J.-I.; Jang, S. Y.; Kwon, S.-J.; and Lee, B. Y., “Tensile Behavior and Cracking Pattern of an Ultra-High Performance Mortar Reinforced by Polyethylene Fiber,” *Advances in Materials Science and Engineering*, V. 2017, 2017, pp. 1-10. doi: 10.1155/2017/5383982

44. Ostergaard, L.; Walter, R.; and Olesen, J. F., “Method for Determination of Tensile Properties of Engineered Cementitious Composites (ECC),” *Proceedings of ConMat’05*, Vancouver, BC, Canada, 2005.

45. Qian, S., and Li, V. C., “Simplified Inverse Method for Determining the Tensile Properties of Strain Hardening Cementitious Composites (SHCC),” *Journal of Advanced Concrete Technology*, V. 6, No. 2, 2008, pp. 353-363. doi: 10.3151/jact.6.353

46. Baby, F.; Graybeal, B.; Marchand, P.; and Touemonde, P., “Proposed Flexural Test Method and Associated Inverse Analysis for Ultra-High-Performance Fiber-Reinforced Concrete,” *ACI Materials Journal*, V. 109, No. 5, Sept.-Oct. 2012, pp. 545-555.

47. Rigaud, S.; Chanvillard, G.; and Chen, J., “Characterization of Bending and Tensile Behavior of Ultra-High Performance Concrete Containing Glass Fibers,” *RILEM Bookseries*, V. 2, 2012, pp. 373-380. doi: 10.1007/978-94-007-2436-5_45

48. López, J. Á.; Serna, P.; Navarro-Gregori, J.; and Camacho, E., “An Inverse Analysis Method Based on Deflection to Curvature Transformation to Determine the Tensile Properties of UHPC,” *Materials and Structures*, V. 48, No. 11, 2015, pp. 3703-3718. doi: 10.1617/s11527-014-0434-0

49. Graybeal, B. A., and Baby, F., “Development of Direct Tension Test Method for Ultra-High-Performance Fiber-Reinforced Concrete,” *ACI Materials Journal*, V. 110, No. 2, Mar.-Apr. 2013, pp. 177-186.

50. AASHTO T 397, “Standard Method of Test for Uniaxial Tensile Response of Ultra-High Performance Concrete,” American Association of State Highway Transportation Officials, Washington, DC, 2022.

51. Huang, H.; Gao, X.; Li, L.; and Huang, H., “Improvement Effect of Steel Fiber Orientation Control on Mechanical Performance of UHPC,” *Construction and Building Materials*, V. 188, 2018, pp. 709-721. doi: 10.1016/j.conbuildmat.2018.08.146

52. Graybeal, B. A., “Compressive Behavior of Ultra-High-Performance Fiber-Reinforced Concrete,” *ACI Materials Journal*, V. 104, No. 2, Mar.-Apr. 2007, pp. 146-152.

53. Graybeal, B. A., and Stone, B., “Compression Response of a Rapid-Strengthening Ultra-High Performance Concrete Formulation,” *TechNote No. FHWA-HRT-12-064*, Federal Highway Administration, McLean, VA, 2012.

54. Smith, G. M., and Young, L. E., “Ultimate Flexural Analysis Based on Stress-Strain Curves of Cylinders,” *ACI Journal Proceedings*, V. 53, No. 12, Dec. 1956, pp. 597-609.

55. ACI Committee 318, “Building Code Requirements for Structural Concrete (ACI 318-19) and Commentary (ACI 318R-19),” American Concrete Institute, Farmington Hills, MI, 2019, 624 pp.

56. Doyon-Barbant, J., and Charon, J. P., “Impact of Fibre Orientation on Tensile, Bending and Shear Behaviors of a Steel Fibre Reinforced Concrete,” *Materials and Structures*, V. 51, No. 6, 2018, p. 157. doi: 10.1617/s11527-018-1282-0

57. Qiu, M.; Zhang, Y.; Qu, S.; Zhu, Y.; and Shao, X., “Effect of Reinforcement Ratio, Fiber Orientation, and Fiber Chemical Treatment on the Direct Tension Behavior of Rebar-Reinforced UHPC,” *Construction and Building Materials*, V. 256, 2020, p. 119311. doi: 10.1016/j.conbuildmat.2020.119311

58. Maya Duque, L. F., and Graybeal, B., “Fiber Orientation Distribution and Tensile Mechanical Response in UHPC,” *Materials and Structures*, V. 50, No. 1, 2017, p. 55. doi: 10.1617/s11527-016-0914-5

APPENDIX I – BACKGROUND

A synopsis of the specified test methods and typical values indicative of UHPC behavior as specified the French, Swiss, and Canadian recommendation documents is presented in **Table A-1**.

Table A-1 –Test methods and typical mechanical properties of structural-grade UHPC according to international recommendations

Property	French standards ^a		Swiss recommendations ^b		Canadian recommendations ^c	
	Test Method	Typ. Values ^d	Test Method	Typ. Values ^d	Test Method	Typ. Values ^d
Density, Kg/m ³ (lb/ft ³)	NF EN 12390-7 ^{e,58}	2300 – 2800 (146 – 175)	SN EN 12390-7 ^{f,59}	2300 – 2700 (146 – 169)	CSA A23.2-6C ^{g,31}	– ^h
Young’s modulus, GPa (ksi)	NF EN 12390-13 ^{e,60}	45 – 65 (6,527 – 9,427)	SN EN 12390-13 ^{f,61}	40 – 60 (5,802 – 8,702)	ASTM C469 ^{g,24}	– ^h
Compressive strength, MPa (ksi)	NF EN 12390-3 ^{e,62}	160 – 230 (23.2 – 33.4)	SN EN 12390-3 ^{f,63}	120 – 200 (17.4 – 29.0)	CSA A23.2-9C ^{g,31}	≥ 120 (≥ 17.4)
Ultimate strain	NF EN 12390-13 ^{e,60}	– ^h	SN EN 12390-13 ^{f,61}	– ^h	ASTM C469 ^{g,24}	0.0035 ⁱ
Poisson’s ratio	NF EN 12390-13 ^{e,60}	0.2 ⁱ	SN EN 12390-13 ^{f,61}	0.2 ⁱ	ASTM C469 ^{g,24}	– ^h
Cracking strength (MPa)	NF P 18-470 ^{i,27}	8 – 12 (1.16 – 1.74)	SIA 2052 ^k	7 – 12 (1.01 – 1.74)	CSA A23.1/S6 ^{l,31}	≥ 5.0 ^m (≥ 0.73)
Localization stress (MPa)	NF P 18-470 ^{i,27}	7 – 12 (1.01 – 1.7)	SIA 2052 ^k	7.7 – 15 (1.12 – 2.18)	CSA A23.1/S6 ^{l,31}	≥ 5.5 ^m (≥ 0.73)
Localization strain	NF P 18-470 ^{i,27}	– ^{h,n}	SIA 2052 ^k	0.0015 – 0.005	CSA A23.1/S6 ^{l,31}	≥ 0.001 ^m

^aAFNOR NF P18-470²⁷ and AFNOR NF P18-710²⁸

^bSIA design guideline 2052²⁹

^cCSA S6:19, Annex A8.1³⁰ and CSA A23.1:19, Annex U³¹, informative (nonmandatory) recommendations

^dTypical mechanical property values at maturity as recommended in each recommendation document; stress and strain typical values may be greater than the specified threshold values to qualify the material for structural use

^eTest method shall be executed with additional provisions listed in Section 5.5 and Annex C of NF P18-470²⁷

^fTest method shall be executed with additional provisions listed in Appendix C of SIA 2052²⁹

^gTest method shall be executed with additional provisions listed in Annex U of CSA A23.1:19³¹

^hTypical value not explicitly stated in recommendation documents

ⁱValues recommended for use in structural design

^jBending test with inverse analysis performed on three- and four-point bending beams according to Annexes D and E of NF P18-470²⁷

^kDirect tension test or four-point bending beam test with inverse analysis performed according to Appendices D and E of SIA 2052²⁹

^lDirect tension test of a published method or four-point flexural prism tested according to ASTM C1609³⁸ with inverse analysis methods of NF P18-470²⁷, SIA 2052²⁹, or Annex A8.1 of CSA S6:19³¹

^mSpecified minimum values for tension hardening behavior

ⁿStrain hardening threshold is imposed on the behavior under flexure. However, the localization strain value is determined from inverse analysis.

Note: 1 ksi = 6.89 MPa

APPENDIX II – EXPERIMENTAL INVESTIGATION

UHPC -Class Materials

The mix design proportions for each UHPC-class material used in this study are shown in **Table A-2**. When several products are provided by the same supplier, each product is assigned a numerical identifier, as shown in **Table A-2**. The manufacturer-reported properties of the fibers used in each UHPC material are listed in **Table A-3**.

Table A-2 –Mixture composition of UHPC-class materials

UHPC supplier	U-A	U-B	U-C	U-D	U-E	U-G	U-H	U-J
Product ID	1	1	1	1; 3 ^c	1	1	1; 2	1
Materials, Kg/m ³								
Premix	2,078 ^a	2086	2,136	2,195	1,920	2,100	2,214; 2179	2,182
Water	165	210	159	130	225	135	166; 174	166
Admixtures	13.7	28.7	— ^d	53.0	44	48	— ^d ; 6.1 ^{d,f}	73.4
Fiber volume content (%)								
1.00	—	—	—	78	—	—	—	—
2.00	164	52/106 ^{b,c}	161	156	156	80/80 ^{b,c}	165; 156	157
2.50	—	—	—	195 ^b	—	—	—	—
3.00	247 ^b	—	—	234	—	—	—	—
3.25	—	85/172 ^c	—	—	254	—	—	—
4.00	—	—	—	312	—	—	—	—
4.50	—	—	363 ^b	—	—	—	—	—
Fiber product								
Fiber supplier	F-A ^g	F-B ^g	F-C ^g	F-D ^g ; G; P; F	F-D ^g	F-E ^g	F-D ^g	F-D ^g
Product line	1	1/2 ^c	1	1	1	1/2 ^c	1	1

^aSupplied as separate ingredient including portland cement, amorphous microsilica, silica sand, and ground quartz flour.

^bSupplier recommended fiber volume fraction.

^cIncluded two types of fiber products reported on the left and right, respectively.

^dThe chemical admixtures were dry powders preblended in the premix.

^eSupplier changed the constituents of the product without modification of the mix proportions.

^fAdditional retarding liquid admixtures were added to preblended dry powder admixtures.

^gUHPC supplier recommended fiber product.

Note: 1 Kg/m³ = 1.686 lb/yd³.

Table A-3 –Fiber properties

Fiber supplier	F-A	F-B	F-C	F-D	F-E	F-F	F-G	F-P		
Product line	1	1	2	1	1	1	2	1	1	1
Material	steel	steel	steel	steel	steel	steel	steel	steel	steel	PVA
Shape	hooked	straight	straight	straight	straight	straight	hooked	straight	straight	straight
Tensile strength (MPa)	1,100	2,100	2,100	2,400	2,600	2,850	2,850	689	2,850	1,000
Length (mm)	30	13	20	13	13	13	25	13	13	12
Cross sectional shape	round	round	round	round	round	round	round	square	round	round
Diameter/width (mm)	0.55	0.3	0.3	0.3	0.2	0.2	0.3	0.43	0.2	0.2

Notes: 1 MPa = 0.145 ksi; 1.00 mm = 0.0394 in.

APPENDIX III – TENSION BEHAVIOR

Tension Response Results

The experimental average of the tensile parameters of the UHPC-class materials tested in this study are listed in **Table A-4** in the imperial system of units.

Table A-4 – Key tension design parameters results for UHPC-class materials (in Imperial system of units).

UHPC ID	Fiber ID	v_f (%)	\bar{f}'_c (ksi)	# of Tests	$\bar{f}_{t,cr}^*$ (ksi)	$\bar{f}_{t,loc}^*$ (ksi)	$\bar{\epsilon}_{t,loc}^*$	Design Model
U-A1	F-A1	2.00	16.20	5	0.69 [5.8%]	0.93 [12.0%]	0.0035 [26.7%]	Bilinear hardening
U-A1	F-A1	3.00	13.89	2	1.07 [1.8%]	1.42 [13.3%]	0.0028 [12.9%]	Bilinear hardening
U-A1	F-A1	3.00	15.20	4	0.99 [10.9%]	1.34 [8.7%]	0.0032 [13.9%]	Bilinear hardening
U-A1	F-A1	3.00	21.39	4	1.13 [6.5%]	1.37 [10%]	0.0029 [25.4%]	Bilinear hardening
U-B1	F-A1/2	2.00	22.21	1	1.1	1.21	0.0036	Elastic-plastic
U-B1	F-A1/2	3.25	14.71	3	1.19 [5.8%]	1.46 [5.7%]	0.0039 [10.6%]	Bilinear hardening
U-D1	F-D1	2.00	24.70	6	1.38 [13.4%]	1.52 [9.4%]	0.0055 [18.8%]	Elastic-plastic
U-D3	F-D1	2.00	13.60	4	1.02 [6.1%]	1.13 [6.4%]	0.0039 [40.5%]	Elastic-plastic
U-D3	F-D1	2.00	18.59	4	1.06 [6.0%]	1.15 [6.5%]	0.0038 [45.4%]	Elastic-plastic
U-D3	F-D1	2.00	22.47	3	1.06 [6.0%]	1.26 [3.8%]	0.0054 [23.8%]	Elastic-plastic
U-D3	F-G1	2.00	21.92	4	1.04 [7.5%]	1.26 [3.3%]	0.0066 [5.2%]	Bilinear hardening
U-D3	F-D1	2.50	14.00	1	1.21	1.32	0.0045	Elastic-plastic
U-D3	F-D1	3.00	12.30	4	1.2 [21.6%]	1.37 [20.2%]	0.0027 [17.6%]	Elastic-plastic
U-D3	F-D1	3.00	13.20	6	1.1 [4.3%]	1.18 [5.6%]	0.0030 [23.7%]	Elastic-plastic
U-D3	F-D1	3.00	17.69	2	1.43 [4.4%]	1.69 [11.1%]	0.0043 [18.6%]	Elastic-plastic
U-D3	F-D1	3.00	18.20	5	1.22 [6.4%]	1.36 [3.6%]	0.0046 [15.8%]	Elastic-plastic
U-D3	F-D1	4.00	14.50	3	1.52 [6.5%]	1.81 [7.1%]	0.0029 [24.5%]	Elastic-plastic
U-D3	F-D1	4.00	18.00	2	1.58 [5.4%]	1.82 [1.1%]	0.0033 [7.4%]	Elastic-plastic
U-E1	F-D1	2.00	13.30	5	0.85 [17.6%]	1.01 [15.9%]	0.0040 [26.6%]	Elastic-plastic
U-E1	F-D1	2.00	17.20	2	1.04 [12.8%]	1.27 [14.5%]	0.0051 [34.1%]	Bilinear hardening
U-E1	F-D1	3.25	14.61	2	1.41 [5.4%]	1.71 [8.1%]	0.0039 [52.4%]	Bilinear hardening
U-E1	F-D1	3.25	17.40	2	1.11 [3.9%]	1.5 [7.4%]	0.0038 [2.1%]	Bilinear hardening
U-G1	F-E1/2	2.00	14.50	3	0.97 [11.3%]	1.19 [9.5%]	0.0064 [20.4%]	Bilinear hardening
U-G1	F-E1/2	2.00	18.80	4	1.16 [14.6%]	1.58 [5.3%]	0.0058 [20.5%]	Bilinear hardening
U-G1	F-E1/2	2.00	20.80	3	1.25 [4.9%]	1.57 [7.3%]	0.0059 [7.4%]	Bilinear hardening
U-H1	F-D1	2.00	16.30	4	1.22 [11.4%]	1.45 [6.1%]	0.0033 [15.2%]	Elastic-plastic
U-H1	F-D1	2.00	23.60	5	1.57 [5.6%]	1.64 [4.8%]	0.0039 [16.9%]	Elastic-plastic
U-H2b	F-D1	2.00	19.90	3	1.52 [8.9%]	1.64 [7%]	0.0037 [4.4%]	Elastic-plastic
U-H2b	F-D1	2.00	20.31	6	1.57 [6.0%]	1.55 [6.7%]	0.0032 [39.8%]	Elastic-plastic
U-J1b	F-D1	2.00	22.10	4	1.29 [12.0%]	1.34 [14.5%]	0.0044 [21.8%]	Elastic-plastic
U-J1b	F-D1	2.00	22.90	3	1.15 [4.6%]	1.25 [9.0%]	0.0052 [9.3%]	Elastic-plastic

* values in brackets represent the coefficient of variation, taken as the ratio of standard deviation to the mean value.

Note: 1 ksi = 6.895 MPa

APPENDIX IV – NOTATION

The following symbols are used in the paper:

E = Modulus of elasticity

f'_c = Compressive strength

ϵ_{cu} = Strain value at maximum compressive strength

ϵ_{cp} = Elastic compressive strain limit utilized in the compression mechanical model

α = Reduction factor applied on the compressive strength

ν = Poisson's ratio

$f_{t,cr}$ = Effective cracking strength

$f_{t,loc}$ = Localization stress when the stress is continuously decreasing with increasing strain

$\epsilon_{t,loc}$ = Localization strain when the stress is continuously decreasing with increasing strain

γ = Reduction factor applied to the effective cracking strength and localization stress

v_f = Fiber content by volume

APPENDIX V –REFERENCES

58. NF EN 12390-7. "Testing of Hardened Concrete - Part 7: Density of Hardened Concrete," *Association Française de Normalization (AFNOR - French Standard Institute)*, 2019.
59. SN EN 12390-7. "Testing Hardened Concrete - Part 7: Density of Hardened Concrete," *Association Française de Normalization (AFNOR - French Standard Institute)*, 2009.
60. NF EN 12390-13. "Testing Hardened Concrete - Part 13: Determination of Secant Modulus of Elasticity in Compression," *Association Française de Normalization (AFNOR - French Standard Institute)*, 2014.
61. SN EN 12390-13. "Testing of Hardened Concrete - Part 13: Determination of Modulus of Elasticity in Compression (Secant Modulus)," *Swiss Association for Standardization*, 2009.

62. NF EN 12390-3. "Testing Hardened Concrete - Part 3: Compressive Strength of Test Specimens," *Association Française de Normalization (AFNOR - French Standard Institute)*, 2012.
63. SN EN 12390-3. "Testing of Hardened Properties - Part 3: Compressive Strength of Test Specimens," *Swiss Association for Standardization*, 2009.